frontiers | Frontiers in Physics

ORIGINAL RESEARCH
published: 14 April 2022
doi: 10.3389/fphy.2022.883319

Ultrafast Laser Direct-Writing of Self-Organized Microstructures in Ge-Sb-S Chalcogenide Glass

Gözden Torun[1]*, *Anupama Yadav*[2†], *Kathleen A. Richardson*[2] *and Yves Bellouard*[1]

[1]Galatea Lab, IEM/STI, Ecole Polytechnique Fédérale de Lausanne (EPFL), Neuchâtel, Switzerland, [2]CREOL and College of Optics and Photonics, University of Central Florida, Orlando, FL, United States

The structuring of mid-IR materials, such as chalcogenide glass (ChG), at the micro and nano scales, is of high interest for the fabrication of photonic devices in general, and for spectroscopy applications in particular. One efficient method for producing regular patterns with a sub-micron to micron length scale is through self-organization processes occurring during femtosecond laser exposure. These processes occur in a broad set of materials, where such self-organized patterns can be found not only on the surface but also within the material volume. This study specifically investigates the case of chalcogenide glass ($Ge_{23}Sb_7S_{70}$) exposed to femtosecond laser pulses, inducing pulse-to-pulse nanostructure formation that is correlated to the glass network structural evolution using Raman spectroscopy as well as morphological and elemental microscopy analysis.

Keywords: chalcogenide glass, NIR femtosecond laser machining, self-organized nanostructures, photo-modifications, nanostructuring, microstructuring

OPEN ACCESS

Edited by:
Matthieu Lancry,
Université Paris-Saclay, France

Reviewed by:
Ciro D'Amico,
Université Jean Monnet, France
Cyril Hnatovsky,
National Research Council Canada (NRC-CNRC), Canada

***Correspondence:**
Gözden Torun
gozden.torun@epfl.ch

***Present Address:**
Anupama Yadav,
Department of Physics, Sri Aurobindo College, University of Delhi, New Delhi, India

Specialty section:
This article was submitted to Optics and Photonics, a section of the journal Frontiers in Physics

Received: *24 February 2022*
Accepted: *25 March 2022*
Published: *14 April 2022*

Citation:
Torun G, Yadav A, Richardson KA and Bellouard Y (2022) Ultrafast Laser Direct-Writing of Self-Organized Microstructures in Ge-Sb-S Chalcogenide Glass. Front. Phys. 10:883319. doi: 10.3389/fphy.2022.883319

INTRODUCTION

There have been numerous efforts to synthesize glass with broad transmission window spanning the mid-and long-wave infrared (MIR and LWIR). Glass systems for these spectral regions are of particular interest not only for vibrational spectroscopy absorption but also for a variety of photonic applications, including optical communications in space [1, 2]. Among MIR and LWIR materials, chalcogenide glass systems are particularly attractive due to their interesting physical and chemical properties [3–5] and their transparency window well above the traditional 2–5 μm spectral range.

Chalcogenide glass (ChG) systems consist of chalcogens from group 6A (S, Se, Te) of the periodic table, which are covalently bonded to other network formers such as As, Ge, Sb, Ga, Si, and P, etc. [6]. As a general condition to complete the coordination number (CN) of the cations, the atomic structure should consist of two bonds for S or Se (CN = 2), three bonds for As or Sb (CN = 3), and four bonds for Ge (CN = 4); such defines the element's bonding configuration in the as-processed glass. Depending on the chalcogen content, homopolar bonds may be found in a particular situation where non-chalcogen metal cations (in this study, Ge) are fully coordinated with chalcogens, and there remains residual S who can only bond to themselves. In glass compositions having higher chalcogen content, this results in chalcogen-chalcogen homopolar bonds. In instances where insufficient chalcogen species are available to fully meet the cation's coordination requirement, one observes metal-metal homopolar bonds [3]. It is the former case that occurs in the compositions studied in this effort, however, an ongoing evaluation in our group is investigating additional response variation when the identity of the iso-structural anion (Se for S), or cation (As for Sb), is changed. This study sets the baseline for our understanding of laser-induced structural changes

TABLE 1 | Physical properties of chalcogenide glasses investigated in this study.

Physical properties (unit)	$Ge_{23}Sb_7S_{70}$
Density (g/cm^3)	2.946 ± 0.001
Thermal diffusivity (m^2/s)	0.2 × 10^{-6}
Transition temperature (Tg, °C)	311 ± 2
Refractive index (at 1.064 μm)	2.25
Band gap (eV)	2.3
Transmission window (μm)	0.593–8.3

occurring during self-organization processes in the ternary glass system where Ge and Sb are fully coordinated and residual S remains forming homopolar bonds [7].

Because of their broad transparency, chalcogenides have prompted investigations on diverse glass compositions since the 1960s [8]. They exhibit a high refractive index, optical nonlinearity with ultrafast response time to the light, photosensitivity, and moderate environmental stability while having low mechanical properties and low glass transition temperature [9]. Their use spans from infrared optical imaging and sensing [10, 11], optical communication systems and photonic devices [5, 6, 12, 13]; laser power delivery [14]; super-continuum generation [15] as well as non-volatile memory and switching devices [16–18]. Over the past decade, various geometries have been explored to expand chalcogenide glass usage, including bulk materials, thin films, and nanoscale waveguides [3–5].

Femtosecond (fs) laser direct-writing is a powerful technique to modify the physical and chemical properties of transparent mediums through nonlinear absorption phenomena. Focused on the surface and/or inside transparent materials, the femtosecond laser can induce diverse and localized permanent morphological and chemical modifications. Self-organized nanogratings [19], crystallization [20], density modulation as well as chemical composition changes [21] due to ions migration are a few examples of reported laser-induced changes in various transparent substrates. For chalcogenide glass, our knowledge about ultrashort laser interaction with these substrates is limited to a few studies [9, 22–39]. Some of the first studies highlight the nonlinear absorption of chalcogenide glass and explore the usage of laser-process thin films as a waveguide [22, 23]. In further studies, reported facts are 1) laser fluence-dependent photo-expansion and a change in refractive index [9, 24–27], 2) surface self-organized nanostructures [28–33], 3) enhanced optical nonlinearity [34–36]. In addition, a few studies explored specifically the laser damage threshold in binary (As-S, As-Se) and ternary (Ge-As-S) chalcogenide glass systems [37–39], primarily for use in fiber-based applications.

In this study, we investigate femtosecond laser-induced modifications in $Ge_{23}Sb_7S_{70}$, manifesting themselves in the form of self-organized nanostructures appearing in the vicinity of its surface, but also, through volume modifications. A Ge-based chalcogenide glass composition was selected for its large glass-forming ability, more rigid glass network, high glass transition, and melting temperature as well as for its technological importance [40]. After the laser exposure, the glass structural evolution after laser exposure was characterized using both transmission measurement and Raman spectroscopy, while its morphological changes were observed using both optical and scanning electron microscopy.

EXPERIMENTAL PROCEDURE

Glass Specimens Preparation and Characterization

The nominal composition of the glass used in this study is $Ge_{23}Sb_7S_{70}$. 100 g of elemental starting materials were weighed and batched in a nitrogen-purged glove box with a controlled atmosphere. The weighed batch was loaded into fused quartz tubes (30 mm in diameter) and sealed under a vacuum using a methane-oxygen torch to form ampoules. The glass batch was melted in a rocking furnace overnight at a melting temperature of 850°C. After overnight rocking at elevated temperature, the molten glass was quenched at 750°C by natural convection. Bulk specimens were subsequently annealed at 270°C for 2 h to relax quench related stresses in the glass.

The density was determined by Archimedes' method with distilled water as immersion fluid at room temperature. The specific heat and thermal conductivity were determined by the transient planar source method. The thermal analysis was performed using a differential scanning calorimeter (DSC from Netzsch DSC 204 F1 Phoenix). The instrument error on temperature was ± 2°C. Transmission data was obtained using Fourier transform infrared spectroscopy (FT-IR from ThermoFisher Scientific Nicolet iS5). Measurements were done over a range of wavelengths from 1.4 to 25 μm on ~4.13 mm thick double-sided polished specimens. Below 1.4 μm, the transmission was measured by UV-VIS-NIR spectrometer. X-ray diffraction (PANalytical Empyrean) was performed to confirm the amorphous nature of the glass. The specimens were cut and polished to optical quality for fs-laser machining. **Table 1** summarizes some of the physical properties of the pristine glass.

Femtosecond Laser Exposure

Three different femtosecond laser systems were used, emitting pulses of different durations: 50 and 100 fs pulses at 850 nm (Yb-doped fiber, Satsuma with an OPA from Amplitude), 150 fs pulses at 1,030 nm (Regen amplifier, S-pulse from Amplitude), and finally, 270 fs pulses also at 1,030 nm (Yb-doped femtosecond fiber laser, Yuzu from Amplitude). This choice of two wavelengths is a compromise for investigating pulse durations, only motivated by the availability of laser sources. Although the 50 and 100 fs pulses are emitted at 850 nm, instead of 1,030 nm like for the other pulse durations, we assume that it remains close enough to 1,030 nm [41, 42], at least for a phenomenological interpretation and discussion. The reasoning is that the wavelength mostly affects the rate of creation of multiphoton seed-electrons, igniting cascading events eventually leading to a plasma formation, mainly sustained by carrier-carrier excitations and avalanche ionization processes. 100 fs pulses were obtained by negatively chirping

the pulse in the compressor, which is the maximum pulse duration in the OPA laser configuration. The specimen was translated under the laser focus with the help of a high-precision motorized stage (Ultra-HR from PI Micos). The laser beam was focused at the surface and in the volume of the specimen with a 0.4-numerical aperture (NA) objective (OFR-20x-1064 nm from Thorlabs), resulting in a spot-size (defined at $1/e^2$) of 1.94 μm for 1,030 nm, 1.6 μm for 850 nm. Note that the focal point is set on the surface, and that, considering our focusing parameters, part of the non-linear interaction volume lies a few microns within the volume. First, static laser exposure was performed to determine the repetition rate at which thermal accumulation outside the exposed volume is observed. Specifically (and following a method proposed in [43]), the transition from non-cumulative to thermal cumulative exposure regime was determined by observing the evolution of the width of the static modifications with the increasing number of pulses and pulse repetition rates from 10 kHz to 1 MHz, for the various laser fluence values. The transition was found around 500 kHz. The repetition rate was then fixed at 100 kHz for most of this study, which lies well below the thermal cumulative regime for this glass. Finally, the laser patterns, consisting of 10 mm-long lines were inscribed at the surface interface, and just below the surface (between 10 and 20 μm) to limit effects related to spherical aberrations (due to the high-index value of the chalcogenide glass). For refractive index measurement, a pattern consisting of a single layer of parallel lines, spaced 2 μm apart and covering a surface of 1×1 mm^2, was written. For absorptivity measurement, a similar pattern was written, this time in the bulk defining an area of 100×100 μm^2 of modified materials. The thickness of this layer written in the volume was defined by the length of the laser-affected zone along the propagation axis and is shown in **Figure 2A**. Writing speed and pulse energy were selected as main variables to vary laser net fluence (or deposited energy). The effective number of pulses (per focal spot) is calculated as

$$M = w_0 \frac{f}{\vartheta} \tag{1}$$

where w_0 defines the beam-waist (defined at $1/e^2$ of the Gaussian intensity distribution) at the focus, f the laser repetition rate (fixed in this case) and ϑ the writing speed, respectively. Accordingly, the laser net fluence on the specimen can be approximated by:

$$E = \frac{4E_p}{\pi w_0}\left(\frac{f}{\vartheta}\right) \tag{2}$$

where E_p is the pulse energy. This laser net fluence represents a dose of how much energy per unit surface is passing through the material in an aperture defined by the beam waist, but does not indicate how much of this energy is effectively absorbed or reflected. While one can achieve the same net fluence either by varying the pulse energy or the writing speed at a fixed repetition rate, the effect may not be the same as the pulse energy also affects the instant peak power level and consequently, the strength of the electrostatic field in the affected zones. However, **Eq. 2** remains a convenient and simple metric for comparing and reproducing experimental exposure conditions from one experiment to another.

Here, pulse-to-pulse overlapping ratios were varied from 0 to 99.9%, and the pulse energy was ranging from 1 nJ to 1 μJ. Furthermore, tracks were inscribed using opposite directions of laser beam movement along with a single writing axis and under three different linear-polarization states (and therefore, the orientation of the electrical field E) defined as parallel, at forty-five degrees, and perpendicular to the writing direction, respectively.

Specimen Characterization

After fs-laser exposure, specimens were first observed using a digital optical microscope with standard lighting conditions (KH-8700 from Hirox). The cross-polarizer optical images were obtained using a polarized light microscope (Olympus BX51). A digital holographic microscope (DHM) was used to measure the optical path differences and subsequently to estimate the refractive index changes at 633 nm.

Specimens having volume modifications were polished to reveal the structures and etched with NaOH (2.5%) for less than 5 s. NaOH has proven itself as an effective etchant for the laser-affected zone for chalcogenide [9]. Specimens coated with a carbon thin film were observed using a field-emission scanning electron microscope (FE-SEM, Gemini 2 from Zeiss) equipped with energy-dispersive X-ray spectroscopy (EDS) operated at 5 kV for high-resolution imaging and 20 kV for elemental analysis. A Raman spectrometer (LabRam HR from Horiba), equipped with a 633 nm-laser excitation source attenuated down to less than 4 mW (to prevent damaging the specimen), was used to record Raman spectra of the modified zones. This wavelength is selected to minimize the absorption in the material. The linearly-polarized Raman laser beam was focused at the surface of the specimen using a 0.9 NA objective (100×-532 nm from Thorlabs). A series of scans were performed at room temperature on each laser-modified zone, with acquisition times of 30 s for each spot.

The transmission and reflection spectra were measured at room temperature for wavelengths ranging from 250 to 2000 nm using an ultraviolet-visible-near-infrared spectrometer (UV-VIS-NIR, Lambda 950 from Perkin Elmer). A mask with a hole of around 1×1 mm^2 is prepared from a black paper for broadband absorbance. For the measurement, the reference beam power is attenuated to 1%, to compensate for the presence of the mask and the ensuing effective drastic reduction of the beam size from the original 2 cm in diameter. The thickness of the sample used for this transmission measurement was 2.5 mm. Finally, the surface roughness was obtained by the laser confocal microscopy (VK-X1000 from Keyence).

RESULTS AND DISCUSSION

Volume Self-Organized Nanostructures

Figure 1 summarizes various regions of modification obtained by dynamic laser exposure in the volume and on the surface as a

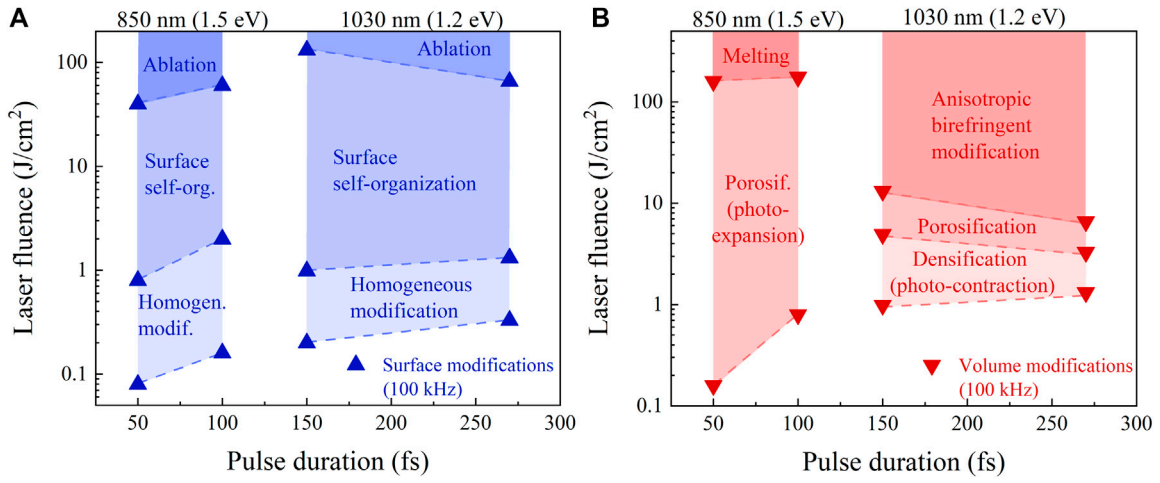

FIGURE 1 | Laser-induced **(A)** volume modifications and **(B)** surface modifications of $Ge_{23}Sb_7S_{70}$ as a function of pulse energy and duration by dynamic laser exposure. The number of effective pulses is fixed to 400, and the repetition rate is 100 kHz.

function of a pulse duration ranging from 50 fs to 270 fs at 100 kHz. For volume modifications, a homogeneous modification was observed at the lowest pulse energy, which subsequently lead to a change in the density and a concurrent increase of refractive index in the glass volume. In fused silica, this regime has been typically observed at low pulse energy and for pulse duration shorter than 200 fs, and it has been linked to localized densification, which results in positive refractive index change as in **Figure 2A** [44–46]. Here, densification was observed at the lowest pulse energy for all the pulse durations considered here.

At relatively higher pulse energies, another regime characterized by the periodic formation of void-like is observed and may be related to the formation of periodic spherical patterns triggered by photo-dissociation processes occurring at higher field densities (**Figure 2C**). Two types of contrast in refractive index as a function of laser fluence have been demonstrated for this glass composition, and relatively similar results in terms of the sign and magnitude were reported for thin-film counterparts as well as for $Ge_{15}As_{15}S_{70}$ [9, 24]. Similarly, the amplitude of change in the refractive index increases with the pulse energy, showing that the glass connectivity progressively decreases with laser fluence. This regime was explained by hydrodynamic expansion followed by thermomechanical relaxation [24]. It has been shown that thermal annealing above glass transition can annihilate the structural changes [24].

The final modification, e.g., densification or porosification, heavily depends on the compactness of the glass network, itself related to the thermal history of the glass [9, 24]. The densification causes photo contraction, whereas porosification results in photo expansion, which has been discussed extensively elsewhere [40, 47]. Densification or porosification alters the refractive index, which was characterized by measuring the optical path difference (OPD) changes (**Supplementary Figure S1**). The densification regime is mostly used to fabricate optical components such as waveguides and diffractive elements; the latter has been used to fabricate micro-lenses [48].

Figure 2 shows the effect of laser processing parameters on the induced morphological changes as visible with a transmission optical microscope. The modifications observed at 100 kHz are mapped in **Figure 1**. Above 500 kHz, in a thermally cumulative regime where heat diffuses away from the focal volume, thermal melting and resolidification occur, leading to the creation of self-organized periodic patterns consisting of single or multiple highly periodic spherical patterns. The repetition rate was fixed at 1 MHz, which lies well within the cumulative regime for chalcogenide glass [40]. As visible in **Figure 2C**, the formation of periodic spherical patterns starts at a pulse energy of 25 nJ, corresponding to an exposure fluence threshold of ~13 J/cm^2. As the laser net fluence is increased, the outer shell of the patterns gets wider, which might be associated with a temperature-driven process. Above 50 nJ (>~165 J/cm^2), a formation of catastrophic fracture, removal of a top surface, and the creation of a crater were observed as shown in **Supplementary Figure S2**, similar to a previous study [49]. Patterns consisting of bubbles with spherical cavities have been demonstrated in fused silica as a consequence of cumulative energy deposition previously [50], but here we did not observe, at least at the scale of our observations, the formation of trapped gas pockets. Further characterization is needed to explore the existence of voids in chalcogenide glasses in the thermal cumulative regime. The self-organized periodic spherical patterns can be used for applications such as 3D data storage, photonic crystals, optical memories, waveguides, gratings, couplers, chemical and/or biological membranes, and other devices [51, 52].

This study specifically investigates the occurrence of self-organized nanostructures consisting of periodically organized parallel nanoplanes, with sub-wavelength periodic features oriented perpendicular to the electric field vector of a linearly polarized femtosecond laser beam. The first occurrence of a self-organization process in glass resulting in nanogratings was

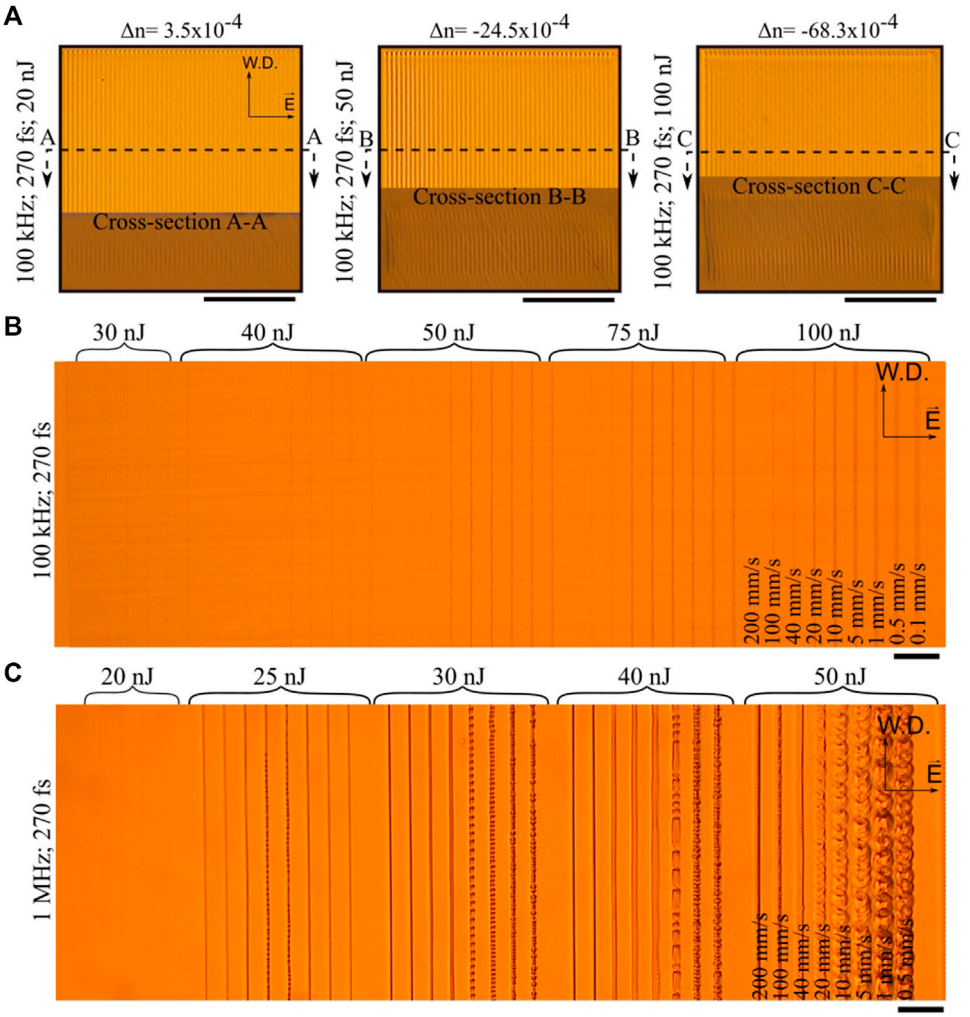

FIGURE 2 | (A) Transmission optical microscope images of 100 × 100 μm^2 laser-modified single plane inscribed with various pulse energies at 100 kHz with a pulse duration of 270 fs The square planes were written 20 μm below the surface. The refractive index changes are estimated based on the optical path difference (OPD) measured by a digital holographic microscope. The standard deviation of the method is estimated to be 2 × 10^{-4}. Transmission optical microscope images of laser inscribed lines with 270 fs-pulses emitted at different repetition rates (lines were written 20 μm below the surface): **(B)** 100 kHz and **(C)** 1 MHz. Scale bars are 40 μm.

reported in fused silica [19]. In this glass system, this type of modification exhibited form-birefringence [53], an increase in etch rate selectivity [54], and stress-induced birefringence [55] resulting from a noticeable localized volume expansion [56]. The nanogratings in fused silica show high thermal stability due to the formation of nanoporous structures as a by-product of the laser-induced decomposition of the glass matrix [57, 58]. From a practical point of view, such modifications have been utilized to produce birefringent and/or monolithic multifunctional devices for 5D optical data storage, micro-optics, photonics, telecommunications, imaging, and so on [59–61]. Like in silica, self-organized nanogratings in this chalcogenide glass studied here are observed inside the glass volume, but also at the glass surface interface, as will be discussed in the next section.

Figures 3A,B show cross-polarizer images of laser-induced modifications at 270 fs, formed in the volume. The polarization anisotropy observed here is attributed to a form-birefringence effect, caused by the existence of periodic structures with alternating refractive index [53].

Figures 3C–G show secondary electron (SE) images of volume modifications for varying laser polarizations. SE images were taken after polishing the specimen surface down to the level of the modifications and subsequently exposed to a flash etching (2.5% NaOH). Even merely polishing the specimen tends to preferentially affect regions of softer material, and thus, distort or possibly erase any small features. In $Ge_{23}Sb_7S_{70}$, this subwavelength periodicity reduces with the pulse energy, from 270 nm at 100 nJ (13 J/mm^2) down to around 220 nm at 200 nJ (26 J/mm^2) at an exposure dose of 400 pulses per spot. The periodicity dependence on the laser fluence as a function of pulse duration is shown in **Supplementary Figure S3**. The formation mechanism of these nanogratings remains unclear.

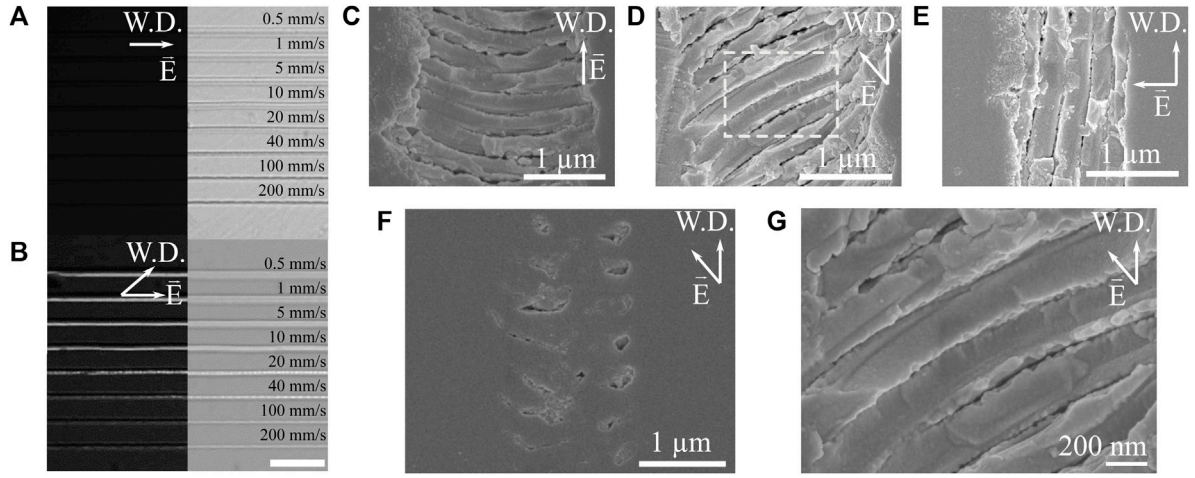

FIGURE 3 | Optical and cross-polarizer images of laser inscribed lines with **(A)** parallel and **(B)** 45-degree polarization orientation with respect to the laser-writing direction. The pulse energy is fixed at 100 nJ. **(C–E)** Secondary electron (SE) images of laser-induced modifications (270 fs pulse length, 100 kHz repetition rate) for three polarization orientations: **(C)** parallel **(D)** 45-degree and **(E)** perpendicular polarization. The pulse energy is 100 nJ with 400 pulses. **(F)** The laser modification with two effective pulses per spot (writing speed of 100 mm/s). **(G)** The higher magnification of the modification in **(D)**.

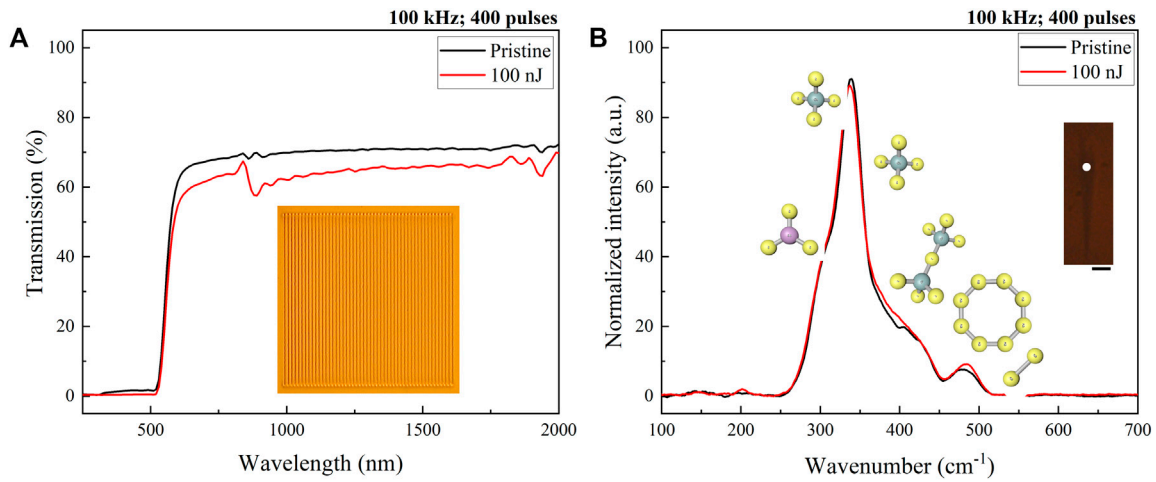

FIGURE 4 | (A) Transmission spectra of the laser-affected zone. The inset shows a reflective optical micrograph of a single plane (1 × 1 mm^2) formed with parallel lines, themselves made of overlapping pulses at 100 nJ. The peaks around 800 nm are measurement artifacts, due to the change of the detector measuring visible to the one measuring NIR during spectral measurement. **(B)** Raman spectra of bulk $Ge_{23}Sb_7S_{70}$ versus laser-induced volume modifications (red curve). Note that the production parameters are similar to the ones reported in **Figure 3C**. The inset image shows the cross-section of the measured laser-affected zone. The scale bar is 4 μm.

To investigate the elemental distribution in the laser affected zone, SEM-EDS was performed. The measured composition of nanogratings was $Ge_{23.2}Sb_{7.1}S_{69.7}$. While near the resolution capability of EDS, the laser-affected zone consists of alternating S-deficient and S-depleted structures. **Figure 4A** shows the transmission spectra of the laser-affected zone in the glass volume. Light-induced defects and the formation of self-organized nanostructures cause a decrease in the transmission spectra notably. The decrease in the transmission is proportional to an increase in reflection as shown in **Supplementary Figure S4A**. Structural changes near these modified regions were also investigated using Raman spectroscopy. Since the Raman laser spot size is around 1 μm at 633 nm, it integrates across the overall bond structure within the full, laser-affected zone, not allowing for a more spatially resolved analysis. However, it does provide some insight into structural changes associated with the laser-induced chemical modification seen by EDS. **Figure 3B** compares Raman spectra of pristine and laser-modified glass. The glass network of $Ge_{23}Sb_7S_{70}$ consists of $GeS_{4/2}$ tetrahedra and

$SbS_{3/2}$ pyramid, which are randomly connected [62]. In addition, S-S bonds are found in S-rich systems, whereas homopolar metal bonds are observed in S-deficient glass systems [63]. Compared to other chalcogenide glass systems, Ge-rich systems have higher thermal stability, thanks to the rigid GeS_4 tetrahedra and to the germanium disulfide (GeS_2) that exhibits a higher glass transition temperature associated with a highly coordinated Ge-backbone [64]. The addition of Ge increases the glass-forming tendency and the melting temperature since GeS_4 tetrahedra has higher effective S-content thus, highly reactive excess sulfur is stabilized. However, the rigidity and compactness of the Ge-S network are reduced by the addition of ternary inclusion (Ga, Sb, etc.) causing a rearrangement of the bond configurations [65]. Previously, it has been shown that the Ge-Sb-S ternary system undergoes structural changes under moderate to intense light sources [65]. This behavior is attributed to coordination defects i.e., dangling bonds and Sb-S bonds.

Figure 4B shows the Raman spectra of laser bulk-modified zone and pristine glass. The spectrum of the pristine glass consists of peaks located between 275 and 485 cm^{-1}. The band at 302 cm^{-1} belongs to SbS_3 pyramids, while 340 cm^{-1} is assigned to GeS_4 tetrahedra [9, 24]. 330 and 402 cm^{-1} are assigned to corner-sharing $GeS_{4/2}$ tetrahedra, and 375 cm^{-1} are attributed to edge-sharing $GeS_{4/2}$ tetrahedra. Two tetrahedra are connected with bridging sulfur, namely $S_3Ge\text{-}S\text{-}Ge_3S$, resulting in a band at 427 cm^{-1}. In addition, excess sulfur causes bands at 475 cm^{-1} as S_8 rings and 485 cm^{-1} as S_n chains [9, 24]. A slight redshift - associated with a decrease in a backbone structure - is observed in the main band of the laser affected zone. These shape and intensity variations of the main band show that the laser-irradiated zone has stronger connectivity (i.e., rapid resolidification causing different network connectivity upon femtosecond laser exposure) than the pristine material. Moreover, a noticeable increase in the band intensity of the S_8 rings, S_n chains, and corner-sharing $GeS_{4/2}$ tetrahedra is observed in the laser affected zone. There is a slight decrease in the bands located at 330 and 340 cm^{-1}. These results indicate the presence of fewer isolated $GeS_{4/2}$ groups and more connectivity of Ge-S-Ge and S-S homopolar bonds. The level of sulfur dissociation as a ring or a chain increases with laser net fluence. As consistent with elemental analysis, we observe a minor decrease in GeS_4 content, whereas Sb_2S_3 content is unaltered. The laser-affected zone shows a random glass network due to local photo-decomposition.

Surface Self-Organized Nanostructures

Figure 1 maps the various modifications in a pulse-duration/pulse-energy space, and qualitatively, shows the general behavior of $Ge_{23}Sb_7S_{70}$ under femtosecond laser irradiation as a function of processing parameters. A *first regime*, observed at the surface and for low pulse energies, consists of apparently homogeneous and continuous structural changes (i.e., zones without obvious heterogeneities visible with the instruments considered in this study).

At higher pulse energies, above this homogeneous regime, a *second regime* consisting of self-organized nanostructures is observed for all pulse durations considered here (i.e., 50 to 270 fs). For the shortest pulse duration (50 fs), self-organized nanostructures are observed in a relatively narrower region compared to the one obtained for longer pulses, while 150 and 270 fs show comparable sizes between themselves. The *surface* self-organization threshold, 1.7 J/cm^2 for a single shot at 100 fs and 1.3 J/cm^2 for a single shot at 270 fs, is two to three times lower than fused silica [66], due to lower bond energy, smaller bandgap, photosensitivity, and higher absorptivity at 1 μm (i.e., the laser wavelength), which is around 25%.

Figure 5 shows secondary electron (SE) images of self-organized nanostructures visible on the glass surface as a function of pulse energy and number of effective pulses per spot. The structures observed have an average subwavelength periodicity of about 250 nm that decreases with the increase of laser fluence (achieved by increasing the number of pulses) down to 170 nm. At higher peak fluence (e.g., above 50 nJ), partial ablation occurs, and randomly distributed spherical nanoparticles with average sizes of 150 nm are found. Traces of nanostructures are observed and, interestingly, in cases for which there is *no overlapping* of two consecutive pulses. The observation of subwavelength periodic structures in *single pulse* exposure is rather specific to chalcogenides [30] and unlike other substrates [66]. **Supplementary Table S1** summarizes the average spatial periodicity of self-organized nanostructures observed on chalcogenide glass surfaces. Interestingly, in some cases, As_2S_3 shows low spatial periodicity (~800 nm) at lower fluence and high spatial periodicity around 200 nm at higher fluence [28–30]. The possible mechanism has been interpreted with the pump-probe experiment previously [28]. The other two glass systems observed are Ge-S and As-Se which show low spatial periodicity around ~750 nm [31, 33]. It suggests that the first step that initiates the self-organization process is driven by the plasma-pulse interaction rather than by pulse-to-pulse accumulation effects. The formation theories of surface self-organized structures in various materials have been summarized with great effort elsewhere [67]. Lower spatial periodicity was explained by surface plasmon wave formation on the surface upon the first shot and the interference phenomenon appears resulting in a redistribution of the laser fluence on the surface. However, the formation of high spatial periodicity remains unclear.

$Ge_{23}Sb_7S_{70}$ glass is known as resistant to oxidation, which might occur during the laser-inscription process, according to similar mechanisms reported in another study [68]. The elemental composition as measured in the self-organized nanostructures shows the composition of nanoplanes in **Figure 5F** as $Ge_{22.5}Sb_{7.7}S_{64.9}O_{4.9}$. SEM-EDS results indicate that the Ge/Sb ratio seems to be slightly affected, that mostly S is removed, and that photo-oxidation is taking place. During fs-laser irradiation, chemical bonds are broken upon the ionization process, and therefore photo-oxidation is a result of trapped oxygen by ionized elements in the ambient conditions. The high sulfur loss might be attributed to low bond energy and high volatility of sulfur.

Figure 6A shows the transmission spectra of both pristine and laser-modified zones. The decrease in the transmission is correlated with an increase in reflection as shown in **Supplementary Figure S4B** and scattering due to surface structures and roughness as in **Supplementary Figure S5**. The transmission decreases with the

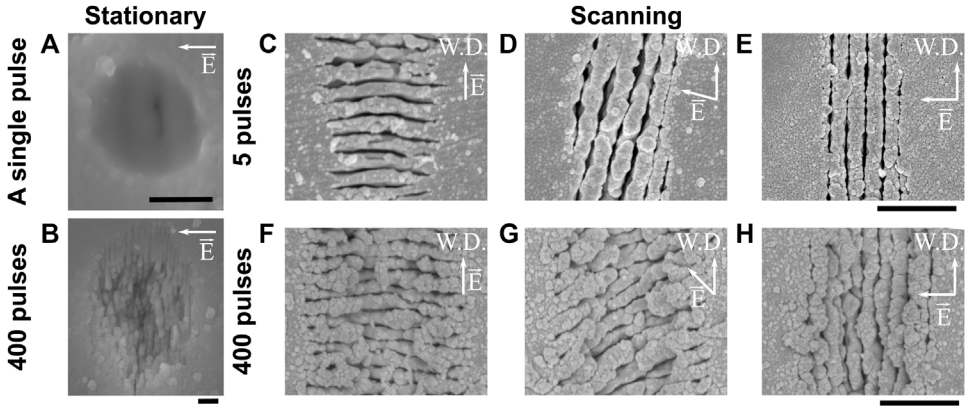

FIGURE 5 | (A,B) SE images of surface self-organized nanostructures on $Ge_{23}Sb_7S_{70}$ under non-scanning conditions. **(A)** a single pulse and **(B)** 400 pulses. **(C–H)** Self-organized nanostructures while scanning along a line at 50 nJ for which 5 pulses overlap and for **(C)** parallel, **(D)** 45°, and **(E)** perpendicular polarization with respect to the writing direction, respectively. Same conditions but this time with 400 pulses overlapping and for **(F)** parallel, **(G)** 45°, and **(H)** perpendicular polarization defined with respect to the writing direction. The scale bar is 1 μm for all images.

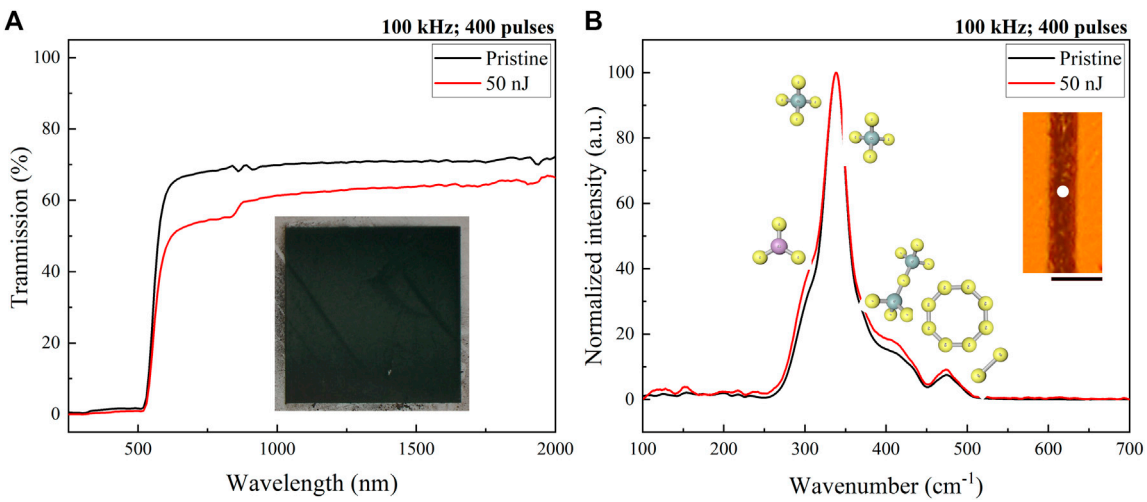

FIGURE 6 | (A) Transmission spectra of pristine and the laser-affected zone of $Ge_{23}Sb_7S_{70}$. The inset shows a reflective optical micrograph of a single plane (1 × 1 mm^2) formed with lines written at 50 nJ with 400 pulses per spot. **(B)** Raman observations of the surface of the pristine and the laser-affected zone of $Ge_{23}Sb_7S_{70}$. In these experiments, the pulse repetition is set to 100 kHz. The inset image shows the measurement point of the laser-affected zone. The scale bar is 4 μm.

pulse energy and is correlated with photo-darkening [26]. The photo-darkening is a rather complex phenomenon, the structural evolution might be helpful for understanding. **Figure 6B** shows the Raman spectra of the pristine glass and the laser-affected zone. Upon ultrafast laser irradiation, both the left and the right shoulder of the main band, related to SbS_3 pyramids at 302 cm^{-1} and corner-sharing $GeS_{4/2}$ tetrahedra at 402 cm^{-1}, respectively, were altered. On one hand, the bands at 302, 330, and 375 cm^{-1} increase with pulse energy whereas, the band at 340 cm^{-1} decreases with the pulse energy. These changes, along with the rise in the intensity of 475 cm^{-1}, indicate the replacement of GeS_4 tetrahedra with edge-sharing and corner-sharing GeS_4 tetrahedra, due to a decaying concentration of sulfur. Overall, the Ge/Sb ratio seems slightly affected by the laser irradiation. On the other hand, by changing the number of pulses, the peak intensity of the right and left shoulders of the main band shows an increase, indicating the onset of glass decomposition. In addition, with both the increasing pulse energy and the number of pulses, the main band was broadened due to the increasing disorder in the glass network [68].

CONCLUSION

We investigated the modifications upon ultrafast laser exposure by varying laser parameters on Ge-based ternary chalcogenide glass ($Ge_{23}Sb_7S_{70}$), both at the surface and in the volume. Various

photo-structural modifications in the volume, ranging from a change in refractive index to the formation of highly periodic spherical patterns were observed. At the lower fluence level, the laser-affected zones display a change in positive and negative refractive index. At higher levels, the formation of self-organized laser patterns, consisting of parallel nanoplanes perpendicular to the laser polarization resembling similar structures found in other glass systems, is observed experimentally, both at and under the surface. The threshold for the onset of this modification was found to be 6.56 J/cm^2 using linearly-polarized 270 fs pulse at 1,030 nm. Similarly, self-organization at the surface was shown with pulse-to-pulse evolution with a threshold of 1.3 J/cm^2. We observed that the magnitude of photo modifications was triggered by the laser fluence. The photo-modified areas at the surface of the glass revealed evidence of photo-oxidation, photo-darkening, and restructuring of the glass network. From the application point of view, these results may enable the direct-write of functional 2.5-dimensional (2.5D) or 3D structures with physical properties tailored with the laser inscription parameters.

DATA AVAILABILITY STATEMENT

The original contributions presented in the study are included in the article/**Supplementary Material**, further inquiries can be directed to the corresponding author.

AUTHOR CONTRIBUTIONS

GT wrote the draft paper and performed most of the experiments presented in this paper, KR and AY did the production and the preliminary characterization of the chalcogenide glass specimens, GT, KR, and YB interpreted the experimental results and analyzed the experimental data. YB designed and supervised the research. All the authors discussed and revised the paper.

ACKNOWLEDGMENTS

The Galatea Lab is thankful to the sponsorship of Richemont International and to University of Central Florida for providing the chalcogenide glass specimens. The authors are thankful to Amplitude for providing one of the experimental femtosecond laser source (OPA) used in this study. The authors would like to thank Dr. Pieter Vlugter for the technical assistance in birefringence and refractive index measurements.

SUPPLEMENTARY MATERIAL

The Supplementary Material for this article can be found online at: https://www.frontiersin.org/articles/10.3389/fphy.2022.883319/full#supplementary-material

REFERENCES

1. Steinmeyer G., Skibina J. S. Entering the Mid-infrared. *Nat Photon* (2014) 8: 814–815. doi:10.1038/nphoton.2014.254
2. Seddon A. B., Tang Z. Q., Furniss D., Sojka Ł., Sakr H., Barney E, et al. Review of Recent Progress towards Mid-infrared Fiber Lasers for 4-9 μm Window. *Adv Photon OSA Tech Dig* (2017). (online) paper NoW2C.1.
3. Adam J.L., Zhang X. *Chalcogenide Glasses: Preparation, Properties and Applications*. Woodhead Publishing Series in Electronic and Optical Materials (2014).
4. Hilton A. R. *Chalcogenide Glasses for Infrared Optics*. McGraw-Hill (2010).
5. Eggleton B. J., Luther-Davies B., Richardson K. Chalcogenide Photonics. *Nat Photon* (2011) 5:141–148. doi:10.1038/nphoton.2011.309
6. Richardson K., Krol D., Hirao K. Glasses for Photonic Applications. *Int. J. Appl. Glass Sci.* (2010) 1:74–86. doi:10.1111/j.2041-1294.2010.00008.x
7. Elliot S.R. *Physics of Amorphous Materials*. Essex: Longman (1990).
8. Frerichs R. New Optical Glasses with Good Transparency in the Infrared**. *J. Opt. Soc. Am.* (1953) 43:1153–1157. doi:10.1364/josa.43.001153
9. Anderson T., Petit L., Carlie N., Choi J., Hu J., Agarwal A, et al. Femtosecond Laser Photo-Response of Ge_23Sb_7S_70 Films. *Opt. Express* (2008) 16: 20081–20098. doi:10.1364/oe.16.020081
10. Adam J-L., Calvez L., Trolès J., Nazabal V. Chalcogenide Glasses for Infrared Photonics. *Int J Appl Glass Sci* (2015) 6:287–294. doi:10.1111/ijag.12136
11. Carlie N., Musgraves J. D., Zdyrko B., Luzinov I., Hu J., Singh V, et al. Integrated Chalcogenide Waveguide Resonators for Mid-IR Sensing: Leveraging Material Properties to Meet Fabrication Challenges. *Opt. Express* (2010) 18:26728–26743. doi:10.1364/oe.18.026728
12. Tao G., Ebendorff-Heidepriem H., Stolyarov A. M., Danto S., Badding J. V., Fink Y, et al. Infrared Fibers. *Adv. Opt. Photon.* (2015) 7:379–458. doi:10.1364/aop.7.000379
13. Li L., Lin H., Qiao S., Zou Y., Danto S., Richardson K, et al. Integrated Flexible Chalcogenide Glass Photonic Devices. *Nat Photon* (2014) 8:643–649. doi:10.1038/nphoton.2014.138
14. Jackson S. D. Towards High-Power Mid-infrared Emission from a Fibre Laser. *Nat Photon* (2012) 6:423–431. doi:10.1038/nphoton.2012.149
15. R. R. Alfano, editor. *The Supercontinuum Laser Source*. 2nd ed. Springer (2006).
16. Harbold J. M., Ilday F. O., Wise F. W., Aitken B. G. Highly Nonlinear Ge-As-Se and Ge-As-S-Se Glasses for All-Optical Switching. *IEEE Photon. Technol. Lett.* (2002) 14(6):822–824. doi:10.1109/LPT.2002.1003105
17. Elliott S. R. Chalcogenide Phase-Change Materials: Past and Future. *Int J Appl Glass Sci* (2015) 6:15–18. doi:10.1111/ijag.12107
18. Hudgens S., Johnson B. Overview of Phase-Change Chalcogenide Nonvolatile Memory Technology. *MRS Bull.* (2004) 29(11):829–832. doi:10.1557/mrs2004.236
19. Shimotsuma Y., Kazansky P. G., Qiu J., Hirao K. Self-organized Nanogratings in Glass Irradiated by Ultrashort Light Pulses. *Phys. Rev. Lett.* (2003) 91: 247405. doi:10.1103/physrevlett.91.247405
20. Torun G., Kishi T., Bellouard Y. Direct-write Laser-Induced Self-Organization and Metallization beyond the Focal Volume in Tellurite Glass. *Phys. Rev. Mater* (2021) 5:055201. doi:10.1103/physrevmaterials.5.055201
21. Fernandez T. T., Sakakura M., Eaton S. M., Sotillo B., Siegel J., Solis J, et al. Bespoke Photonic Devices Using Ultrafast Laser Driven Ion Migration in Glasses. *Prog Mater Sci* (2018) 94:68–113. doi:10.1016/j.pmatsci.2017.12.002
22. Fazio E., Hulin D., Chumash V., Michelotti F., Andriesh A. M., Bertolotti M. On-off Resonance Femtosecond Non-linear Absorption of Chalcogenide Glassy Films. *J Non-Crystalline Sol* (1994) 168(3):213–222. doi:10.1016/0022-3093(94)90332-8
23. Miura K., Qiu J., Inouye H., Mitsuyu T., Hirao K. Photowritten Optical Waveguides in Various Glasses with Ultrashort Pulse Laser. *Appl. Phys. Lett.* (1997) 71:3329–3331. doi:10.1063/1.120327
24. D'Amico C., Caillaud C., Velpula P. K., Bhuyan M. K, Somayaji M., Colombier J-P, et al. Ultrafast Laser-Induced Refractive index Changes in $Ge_{15}As_{15}S_{70}$ Chalcogenide Glass. *Opt. Mater. Express* (2016) 6:1914–1928. doi:10.1364/OME.6.001914
25. David Musgraves J., Carlie N., Petit L., Boudebs G., Choi J., Richardson M, et al. Effect of Replacement of as by Ge and Sb on the Photo-Response under

Near Infrared Femtosecond Laser Irradiation in As-Based Sulfide Glasses. *Int J Appl Glass Sci* (2011) 2:308–320. doi:10.1111/j.2041-1294.2011.00060.x
26. Petit L., Carlie N., Anderson T., Couzi M., Choi J., Richardson M, et al. Effect of IR Femtosecond Laser Irradiation on the Structure of New Sulfo-Selenide Glasses. *Opt Mater* (2007) 29:1075–1083. doi:10.1016/j.optmat.2006.04.008
27. Gecevičius M, Beresna M, Zhang J, Yang W, Takebe H, Kazansky PG. Extraordinary Anisotropy of Ultrafast Laser Writing in Glass. *Opt. Express* (2013) 21:3959–68. doi:10.1364/OE.21.003959
28. Yu X., Qi D., Wang H., Zhang Y., Wang L., Zhang Z, et al. *In Situ* and *Ex-Situ* Physical Scenario of the Femtosecond Laser-Induced Periodic Surface Structures. *Opt. Express* (2019) 27:10087–10097. doi:10.1364/oe.27.010087
29. Yu X., Zhang Q., Qi D., Tang S., Dai S., Zhang P, et al. Femtosecond Laser-Induced Large Area of Periodic Structures on Chalcogenide Glass via Twice Laser Direct-Writing Scanning Process. *Opt Laser Technology* (2020) 124: 105977. doi:10.1016/j.optlastec.2019.105977
30. Zhang Q., Lin H., Jia B., Xu L., Gu M. Nanogratings and Nanoholes Fabricated by Direct Femtosecond Laser Writing in Chalcogenide Glasses. *Opt. Express* (2010) 18:6885–6890. doi:10.1364/oe.18.006885
31. Messaddeq S. H., Vallée R., Soucy P., Bernier M., El-Amraoui M., Messaddeq Y. Self-organized Periodic Structures on Ge-S Based Chalcogenide Glass Induced by Femtosecond Laser Irradiation. *Opt. Express* (2012) 20(28): 29882–29889. doi:10.1364/oe.20.029882
32. Messaddeq S. H., Dumont A., Douaud A., El-Amraoui M., Messaddeq Y. Formation of Cross-Superposed LIPSSs on Bulk Chalcogenide Glasses Using Fs-Laser. *Adv Opt Tech* (2018) 7(5):311–319. doi:10.1515/aot-2018-0031
33. Zhang Y., Xu Y., Zhang P., You C., Zhang S., Xie M, et al.Femtosecond-laser-induced Submicron Grating Periodic Structures on As2S3 and As35Se65 Glasses. *Opt Laser Technology* (2018) 108:306–309. doi:10.1016/j.optlastec.2018.07.002
34. Choi J. W., Han Z., Sohn B-U., Chen G. F. R., Smith C., Kimerling L. C, et al. Nonlinear Characterization of GeSbS Chalcogenide Glass Waveguides. *Sci Rep* (2016) 6:39234. doi:10.1038/srep39234
35. Sohn B-U., Kang M., Choi J. W., Agarwal A. M., Richardson K., Tan D. T. H. Observation of Very High Order Multi-Photon Absorption in GeSbS Chalcogenide Glass. *APL Photon* (2019) 4:036102. doi:10.1063/1.5085504
36. Hu Y., Tian K., Li T., Zhang M., Ren H., Qi S, et al. Mid-infrared Nonlinear Optical Performances of Ge-Sb-S Chalcogenide Glasses. *Opt. Mater. Express* (2021) 11:695–706. doi:10.1364/ome.412731
37. Long N., Xia M., Zhang P., Nie Q., Xu Y. Effect of Chemical Composition on the Structure, Optical Properties and Femtosecond Laser Ablation Performance of Ge-Sb-Se Glasses. *J Alloys Compounds* (2019) 779:543–549. doi:10.1016/j.jallcom.2018.11.058
38. Zhu L., Yang D., Wang L., Zeng J., Zhang Q., Xie M, et al. Optical and thermal Stability of Ge-As-Se Chalcogenide Glasses for Femtosecond Laser Writing. *Opt Mater* (2018) 85:220–225. doi:10.1016/j.optmat.2018.08.041
39. Zhang M., Li T., Yang Y., Tao H., Zhang X., Yuan X, et al. Femtosecond Laser Induced Damage on Ge-As-S Chalcogenide Glasses. *Opt. Mater. Express* (2019) 9(2):555–561. doi:10.1364/ome.9.000555
40. Anderson T. P. *Fabrication of Integrated Optofluidic Circuits in Chalcogenide Glass Using Femtosecond Laser Direct Writing* (2010). Thesis 1518 https://stars.library.ucf.edu/etd/1518.
41. Simanovskii D. M., Schwettman H. A., Lee H., Welch A. J. Midinfrared Optical Breakdown in Transparent Dielectrics. *Phys. Rev. Lett.* (2003) 91:107601. doi:10.1103/physrevlett.91.107601
42. Ji T. Q., Chen H. X., Huang M., Zhao F. L., Li SX. X., Xu Z, et al. Ultraviolet-infrared Femtosecond Laser-Induced Damage in Fused Silica and CaF_2 Crystals. *Phys. Rev. B* (2006) 73:054105. doi:10.1103/physrevb.73.054105
43. Schaffer C. B., García J. F., Mazur E. Bulk Heating of Transparent Materials Using a High-Repetition-Rate Femtosecond Laser. *Appl Phys A: Mater Sci Process* (2003) 76:351–354. doi:10.1007/s00339-002-1819-4
44. Hnatovsky C., Taylor R. S., Rajeev P. P., Simova E., Bhardwaj V. R., Rayner D. M, et al. Pulse Duration Dependence of Femtosecond-Laser-Fabricated Nanogratings in Fused Silica. *Appl. Phys. Lett.* (2005) 87:014104. doi:10.1063/1.1991991
45. Bellouard Y., Barthel E., Said A. A., Dugan M., Bado P. Scanning thermal Microscopy and Raman Analysis of Bulk Fused Silica Exposed to Lowenergy Femtosecond Laser Pulses. *Opt. Express* (2008) 16(24):19520–19534. doi:10.1364/oe.16.019520
46. Lapointe J., Bérubé J-P., Pouliot S., Vallée R. Control and Enhancement of Photo-Induced Refractive index Modifications in Fused Silica. *OSA Continuum* (2020) 3:2851–2862. doi:10.1364/osac.406247
47. Calvez L., Yang Z., Lucas P. Reversible Giant Photocontraction in Chalcogenide Glass. *Opt. Express* (2009) 17:18581–18589. doi:10.1364/oe.17.018581
48. Knotek P., Tichy L. On Photo-Expansion and Microlens Formation in (GeS_2) $0.74(Sb_2S_3)0.26$ Chalcogenide Glass. *Mater Res Bull* (2012) 47:12 4246–4251. doi:10.1016/j.materresbull.2012.09.024
49. Juodkazis S., Misawa H., Louchev O. A., Kitamura K. Femtosecond Laser Ablation of Chalcogenide Glass: Explosive Formation of Nano-Fibres against Thermo-Capillary Growth of Micro-spheres. *Nanotechnology* (2006) 17: 4802–4805. doi:10.1088/0957-4484/17/19/003
50. Bellouard Y., Hongler M-O. Femtosecond-laser Generation of Self-Organized Bubble Patterns in Fused Silica. *Opt. Express* (2011) 19:6807–6821. doi:10.1364/oe.19.006807
51. Graf R., Fernandez A., Dubov M., Brueckner H. J., Chichkov B. N., Apolonski A. Pearl-chain Waveguides Written at Megahertz Repetition Rate. *Appl. Phys. B* (2007) 87(1):21–27. doi:10.1007/s00340-006-2480-y
52. Ma H., Zakoldaev R. A., Rudenko A., Sergeev M. M., Veiko V. P., Itina T. E. Well-controlled Femtosecond Laser Inscription of Periodic Void Structures in Porous Glass for Photonic Applications. *Opt. Express* (2017) 25:33261–33270. doi:10.1364/oe.25.033261
53. Bricchi E., Klappauf B. G., Kazansky P. G. Form Birefringence and Negative index Change Created by Femtosecond Direct Writing in Transparent Materials. *Opt. Lett.* (2004) 29:119–121. doi:10.1364/ol.29.000119
54. Hnatovsky C., Taylor R. S., Simova E., Bhardwaj V. R., Rayner D. M., Corkum P. B. Polarization-selective Etching in Femtosecond Laser-Assisted Microfluidic Channel Fabrication in Fused Silica. *Opt. Lett.* (2005) 30: 1867–1869. doi:10.1364/ol.30.001867
55. Bellouard Y., Colomb T., Depeursinge C., Dugan M., Said A. A., Bado P. Nanoindentation and Birefringence Measurements on Fused Silica Specimen Exposed to Low-Energy Femtosecond Pulses. *Opt. Express* (2006) 14(18): 8360–8366. doi:10.1364/oe.14.008360
56. Champion A., Bellouard Y. Direct Volume Variation Measurements in Fused Silica Specimens Exposed to Femtosecond Laser. *Opt. Mater. Express* (2012) 2: 789–798. doi:10.1364/ome.2.000789
57. Lancry M., Poumellec B., Canning J., Cook K., Poulin J-C., Brisset F. Ultrafast Nanoporous Silica Formation Driven by Femtosecond Laser Irradiation. *Laser Photon Rev* (2013) 7:953–962. doi:10.1002/lpor.201300043
58. Wang Y., Lancry M., Cavillon M., Poumellec B. Lifetime Prediction of Nanogratings Inscribed by a Femtosecond Laser in Silica Glass. *Opt. Lett.* (2022) 47:1242–1245. doi:10.1364/ol.449486
59. McMillen B., Athanasiou C., Bellouard Y. Femtosecond Laser Direct-Write Waveplates Based on Stress-Induced Birefringence. *Opt. Express* (2016) 24: 27239–27252. doi:10.1364/oe.24.027239
60. Zhang J, Gecevičius M, Beresna M, Kazansky PG. Seemingly Unlimited Lifetime Data Storage in Nanostructured Glass. *Phys. Rev. Lett.* (2014) 112: 033901. doi:10.1103/PhysRevLett.112.033901
61. Bellini N., Vishnubhatla K. C., Bragheri F., Ferrara L., Minzioni P., Ramponi R, et al. Femtosecond Laser Fabricated Monolithic Chip for Optical Trapping and Stretching of Single Cells*Opt. Express* (2010) 18:4679–4688. doi:10.1364/oe.18.004679
62. Musgraves J. D., Carlie N., Hu J., Petit L., Agarwal A., Kimerling L. C, et al. Comparison of the Optical, thermal and Structural Properties of Ge-Sb-S Thin Films Deposited Using thermal Evaporation and Pulsed Laser Deposition Techniques. *Acta Materialia* (2011) 59(12):5032–5039. doi:10.1016/j.actamat.2011.04.060
63. Petit L., Carlie N., Chen H., Gaylord S., Massera J., Boudebs G, et al. Compositional Dependence of the Nonlinear Refractive index of New Germanium-Based Chalcogenide Glasses. *J Solid State Chem* (2009) 182: 2756–2761. doi:10.1016/j.jssc.2009.07.027
64. Nathan C. *A Solution-Based Approach to the Fabrication of Novel Chalcogenide Glass Materials and structuresPhD Dissertation*. Clemson University (2010).
65. Yadav A., Kang M., Kang M., Smith C., Lonergan J., Buff A, et al. Influence of Phase Separation on Structure-Property Relationships in the (GeSe2-3As2Se3) 1−xPbSex Glass System. *Phys. Chem. Glasses: Eur. J. Glass Sci. Technol. B* (2017) 58(4):115–126. doi:10.13036/17533562.58.4.115

66. Liang F., Vallée R., Chin S. L. Mechanism of Nanograting Formation on the Surface of Fused Silica. *Opt. Express* (2012) 20:4389–4396. doi:10.1364/oe.20.004389
67. Bonse J., Gräf S. Maxwell Meets Marangoni-A Review of Theories on Laser-Induced Periodic Surface Structures. *Laser Photon Rev* (2020) 14:2000215. doi:10.1002/lpor.202000215
68. Tanaka K. Photo-induced Phenomena in Chalcogenide Glasses: Comparison with Those in Oxide Glass and Polymer. *J Non-Crystalline Sol* (2006) 352(23–25):2580–2584. doi:10.1016/j.jnoncrysol.2006.02.070

Conflict of Interest: The authors declare that the research was conducted in the absence of any commercial or financial relationships that could be construed as a potential conflict of interest.

Publisher's Note: All claims expressed in this article are solely those of the authors and do not necessarily represent those of their affiliated organizations, or those of the publisher, the editors and the reviewers. Any product that may be evaluated in this article, or claim that may be made by its manufacturer, is not guaranteed or endorsed by the publisher.